Topological aspects of the structure of chaotic attractors in $\mathbb{R}^3$

Tsvetelin D. Tsankov and Robert Gilmore
Department of Physics, Drexel University, Philadelphia, Pennsylvania 19104, USA
(Received 13 November 2003; published 12 May 2004)

Strange attractors with Lyapunov dimension $d_L<3$ can be classified by branched manifolds. They can also be classified by the bounding tori that enclose them. Bounding tori organize branched manifolds (*classes* of strange attractors) in the same way as the branched manifolds organize the periodic orbits in a strange attractor. We describe how bounding tori are constructed and expressed in a useful canonical form. We present the properties of these canonical forms and show that they can be uniquely coded by analogs of periodic orbits of period $g-1$, where g is the genus. We describe the structure of the global Poincaré surface of section for an attractor enclosed by a genus-g torus and determine the transition matrix for flows between the $g-1$ components of the Poincaré surface of section. Finally, we show how information about a bounding torus can be extracted from scalar time series.

DOI: 10.1103/PhysRevE.69.056206 PACS number(s): 05.45.Ac

I. INTRODUCTION

Obtaining a global, qualitative understanding of the structure of chaotic attractors in dissipative dynamical systems must be pursued using topological methods. Only in this way can we uncover general properties that are common to a large class of systems and are invariant under continuous deformations that are orientation preserving diffeomorphisms. Once obtained, such knowledge can be best utilized by constructing a classification scheme for chaotic attractors which is of immense importance for the maturity of the field of nonlinear dynamics.

We have recently proposed a new tool—bounding tori—as a means for classifying low-dimensional strange attractors [1]. These are strange attractors that can be embedded in $\mathbb{R}^3$, whose Lyapunov dimension d_L is less than three. The purpose of this work is to provide information about how these bounding tori are constructed, what their properties are, and how they are used. In Sec. II we provide background information to show how this new tool is related to the topological tools that we have previously introduced to classify and analyze low-dimensional strange attractors. These tools are relative rotation rates [2], branched manifolds [3], and basis sets of orbits [4]. In Sec. III we discuss in detail how bounding tori are constructed for a well-known strange attractor—the Lorenz attractor. In particular, we describe how the bounding torus is expressed in a particular canonical form. In Sec. IV we discuss canonical forms and their general properties. Canonical forms allow us to provide a precise answer to a difficult question: "What is the structure of the Poincaré surface of section for a strange attractor?" The Poincaré surface of section has $g-1$ disconnected components when the strange attractor can be enclosed in a torus with $g\geqslant 3$ holes (genus-g surface). This is shown in Sec. V. In the following section we construct transition matrices describing how the flow distributes initial conditions on each component to the other components of the Poincaré section. In Sec. VII we introduce three different but related ways to classify canonical forms. Each involves an orbit of period $g-1$. All canonical forms up to $g=9$ are listed in Sec. VIII. Procedures for extracting information about the canonical form from experimental data are presented, along with an example, in Sec. IX. Our results are summarized in the concluding section.

II. BACKGROUND

Even in low-dimensional dynamical systems we find a very rich variety of possible structures due to an intricate interplay between topology and dynamics. In this paper we deal exclusively with chaotic attractors in $\mathbb{R}^3$ with Lyapunov exponents $\lambda_1>0, \lambda_2=0, \lambda_3<0$ and Lyapunov dimension $d_L=2+\lambda_1/|\lambda_3|<3$. In phase space $\mathbb{R}^3$ we can rely on a large set of important results from topology to construct a classification scheme. In Ref. [1] we laid out the foundations of the third coarsest level of a classification scheme, for which the first two levels have already been completed [5,6]. At the finest level strange attractors are classified by a basis set of orbits [4]. This is defined as follows: for every finite period there exists a finite set of unstable periodic orbits embedded with the attractor that forces the existence of all the other unstable periodic orbits. At the intermediate level there is a classification by branched manifolds. Branched manifolds serve as periodic orbit organizers. They are built from two basic structures—splitting and joining charts. These charts represent the two basic processes—stretching and squeezing—that act in phase space to produce chaotic behavior, generate strange attractors, and organize all the unstable periodic orbits in the strange attractor in a unique way. Splitting and joining charts are connected in such a way that there are no free ends. Their connected union forms a compact two-dimensional structure with boundary. It is a manifold everywhere except at the singularities of the charts—branch lines for the joining charts and splitting points for the splitting charts.

Branched manifolds (also known as templates or knot holders) were first introduced by Birman and Williams [7] to facilitate the study of the topological organization of knotted and linked periodic orbits for flows in $\mathbb{S}^3$. Their work found an immediate application in the study of chaotic attractors in three-dimensional dynamical systems but the results apply

directly only to hyperbolic strange attractors. The hyperbolic limit has never been observed either in experiments or in numerical solutions of systems of ordinary differential equations (ODEs). The extension of the branched manifold approach to nonhyperbolic strange attractors can be done via the mechanism of basis set of orbits described above. In the nonhyperbolic case we in general see fewer unstable periodic orbits in the flow than predicted by the template. The orbits that are present are organized exactly as the orbits in the template (the same set of linking numbers). To characterize the set of orbits actually present in the flow we need to specify the basisset of orbits. Different chaotic attractors can be characterized by the same branched manifold but different basis sets. This is the relation between the first two levels of the classification scheme.

In this paper we explore the possibility for construction of a third level of classification. It is based on canonical forms—planar surfaces with nonzero genus and dressed with one-dimensional flow reflecting the nature of the singularities in the branched manifold. These planar surfaces are introduced in a formal way as follows. First we introduce an embedding manifold for the strange attractor (and its branched manifold). This is not something preexisting in phase space with certain size and it should not be confused with domain of attraction. It is a specifically constructed compact orientable three-manifold with boundary. The boundaries are well known and classified surfaces—tori with genus 1 or higher. The purpose of such an embedding manifold is to "enclose" the strange attractor and isolate it from the fixed points of the flow. The global topological structure of the chaotic attractor is determined to a large extent by the type and location in phase space of such fixed points [8]. The existence of fixed points in the flow leads to the robust presence of holes in the body of the attractor. In addition to this there is also a set of singularities for the flow when restricted to the boundary surface of the embedding manifold. The number of these singularities reflects not only the genus of the surface but also the number of singular sets for the branched manifold. At the next step, following a formal procedure, we introduce a special type of planar surface called a canonical form, which is a simplified record of the genus of the embedding manifold and the singularities on its boundary. It turns out that canonical forms have a very rich but rigid organization and are ideally suited for classifying branched manifolds. In addition, in the same way as the knot holders are orbit organizers we can say that embedding manifolds and their canonical forms are knot holder organizers—many different branched manifolds with the same set of singularities but different number of branches can live inside the same embedding manifold.

In support of our idea to use embedding manifolds we would like to make the following remark. This is the most natural context in which concepts from algebraic topology such as homology groups and homotopy groups can be introduced to provide a hint at the global structure of the attractor. There have been some attempts in the literature to introduce the notion of homology groups for a strange attractor [9,10]. We prefer to use an indirect correspondence since this way the question of precise mathematical definition of the properties of a strange attractor as a topological space is avoided. Dealing with well-defined smooth topological objects is preferable.

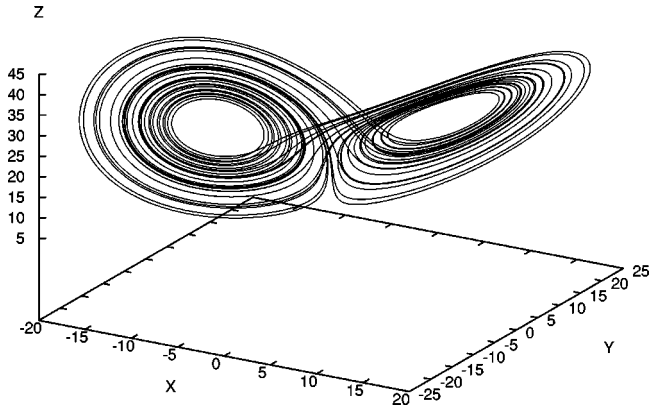

FIG. 1. Solution of the Lorenz system of ODEs approaching a strange attractor. Control parameter values: $(\sigma,r,b)=(10,28,8/3)$.

III. EXAMPLE—THE LORENZ SYSTEM

To illustrate our approach we provide one example. It is the well-known Lorenz system of ODEs [11]. The equations are

$$\dot{x} = -\sigma(x-y),$$

$$\dot{y} = rx - y - xz,$$

$$\dot{z} = -bz + xy. \tag{1}$$

A solution approaching the strange attractor is computed numerically for parameter values $(\sigma,r,b)=(10,28,8/3)$ and is plotted in Fig. 1. The system is dissipative everywhere in phase space. For the parameter values listed above there are three fixed points. There is a saddle fixed point at the origin. The linearized system about this point has two real negative and one positive eigenvalues. The equations are invariant under the discrete rotation group $R_z(\pi)$ and the z axis is part of the stable manifold of the saddle fixed point. There are also two symmetrically placed fixed points. They are unstable foci—the linearized system about each of them has one real negative eigenvalue and two complex conjugate eigenvalues with positive real part. All solutions of the Lorenz system remain bounded for all time. Solutions originating far away from the origin are attracted asymptotically to an ellipsoid in phase space containing the strange attractor and the three fixed points [11]. From a topological point of view this ellipsoid is a three-dimensional ball whose boundary is a two-dimensional sphere.

Next we carry out a construction that is common in topology—starting from a given topological space we turn it into a different space by removing certain regions in it. First we remove the fixed points from the ellipsoid (the ball). Next we remove one-dimensional invariant manifolds of the fixed points that extend globally and intersect the bounding two-sphere of the ball. For the two foci this means a removal of their one-dimensional stable manifolds, and for the saddle

point at the origin elimination of the z axis altogether. In fact the stable (two-dimensional) manifold of the fixed point at the origin has a very complex structure that has profound influence on the behavior of chaotic solutions. We can, however, delete the z axis from it on the premises that solutions starting on the z axis remain there forever—nothing interesting happens. Thus we started with a three-ball containing the attractor and the fixed points, and then we drill holes in it along the one-dimensional stable invariant manifolds through the fixed points that intersect the boundary of the attracting ellipsoid. This turns the ellipsoid into a solid block with three holes. The technical term for such an object is a handle-body of genus 3. The boundary of this three-manifold is a closed orientable two-dimensional surface—a torus with genus 3. This boundary is a trapping surface in some rather loose sense—all solutions starting on the outside of the handle-body and tending to the chaotic attractor cross the boundary in finite time, from the outside to the inside, and never escape from the interior. Note that parts of the invariant manifolds of the saddle fixed point at the origin still exist inside the handle-body.

By the above construction we establish a formal correspondence between the chaotic attractor for the Lorenz system and an embedding three-manifold (a handle-body) that is bounded by a torus with genus 3. This may seem rather arbitrary at this stage but it is not entirely unjustified since it is based not only on topological considerations but also on dynamical ones. To provide an alternative view, next we look at the branched manifold associated with the chaotic attractor of the Lorenz system.

First, we start with the branched manifold given in the usual "mask" representation—it is shown at the top of Fig. 2. Note that in this representation the branch line is degenerate—the semiflow upon crossing it is redirected into two different regions of the branched manifold. It is possible to split the branch line in two and "slide" the pieces around the circular holes in the template. This is an example of a branched manifold transformation called a local move. The possible local moves are discussed in Ref. [6]. In the next stages we extend the splitting point backwards and then give the right branch line a half twist. The result is a branched manifold as shown at the bottom of Fig. 2.

Note that in the final form of the template, when viewed in this projection on the plane, the semiflow goes around the circular holes in the same direction—clockwise. Now we can "blow up" the resulting branched manifold back to a three-manifold. This is done by surrounding each point in the branched manifold by a small three-dimensional ball of radius ϵ and taking the union of these balls. It is clear that in this case the resulting space has the topology of a handle-body of genus 3; this is consistent with our previous conclusion. All branched manifolds in Fig. 2 describe the same topological organization of periodic orbits and thus they correspond to chaotic attractors that are related by orientation preserving diffeomorphisms.

Now let us go back to the original phase space and consider what happens when the flow crosses the torus that bounds the embedding handle-body. We assume that the boundary is a smooth surface. This can always be achieved since we allow ourselves to modify the boundary any way we wish, provided we do not change the genus. If the handle-body is $\mathcal{H}B$, its boundary is $\partial\mathcal{H}B$. At each point on the boundary we can decompose the flow into a tangential $\vec{v}_{\parallel}$ and a normal $\vec{v}_{\perp}$ component. The normal component never vanishes since the flow goes into the bounded region. The tangential component could be zero and this leads to a fixed point for the surface flow. The Euler characteristic for the torus with genus $g=3$ is $\chi=2-2g=-4$. A well-known theorem from topology—the Poincaré-Hopf Index Theorem [12]—relates the sum of the indices evaluated at all fixed points i of the flow restricted to the surface to the Euler characteristic of the surface:

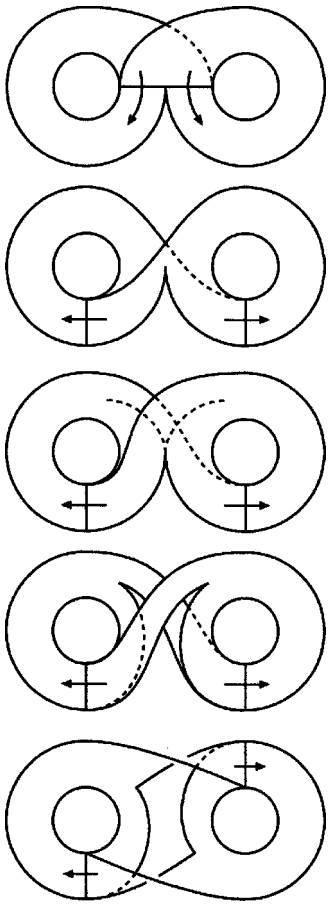

FIG. 2. Transformation of the branched manifold for the Lorenz system into a different form by applying a series of local moves.

$$\chi(\partial\mathcal{H}B)=\sum_{i=1}^{n}\mathrm{ind}_i(\vec{v}_{\parallel}). \tag{2}$$

The fixed points for the surface flow can only be saddles due to the fact that there is one positive and one negative Lyapunov exponent in directions transverse to the flow. The index of each fixed point for the surface flow is $(-1)^{n_u}$, where n_u is the number of unstable directions for the flow. In our case the index can be only -1. We have a total of four saddle points for the surface flow on the torus bounding the branched manifold at the bottom of Fig. 2. The singularities on the genus-3 surface enclosing the branched manifold

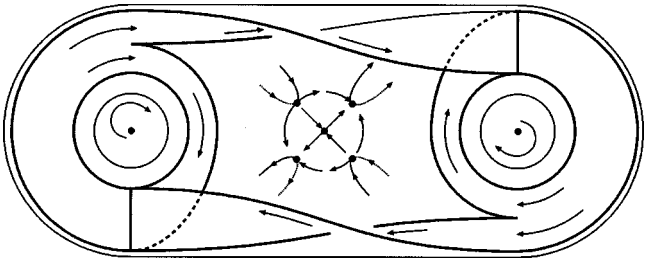

FIG. 3. The branched manifold at the bottom of Fig. 2 is shown enclosed by a bounding torus of genus 3. All three fixed points in the vector field generating the flow are outside the bounding torus. The flow around the two foci, as well as the regular saddle that separates them, is shown. The four singularities on the surface induced by the flow in the neighborhood of the central hole are shown as dots and the flow directions in the neighborhood of these four singularities are shown. All four singularities are regular saddles.

shown at the bottom of Fig. 2 are shown in Fig. 3. Note also that the branched manifold has four singular sets—two branch lines and two splitting points. This shows that there is some relation between the singular sets of the branched manifold and the fixed points for the flow on the surface of the bounding torus. Thus we are led to look for some convenient way to express this relation.

We now propose an algorithm for constructing this canonical form. First, in the original phase space we construct a smooth surface Σ that is an embedding of a two-dimensional disk in $\mathbb{R}^3$. Apart from being orientable and bounded by a topological circle, the surface is constructed so that the following conditions are true:

(1) It contains the two unstable focal points.

(2) The two-dimensional unstable manifolds of the focal points are tangent to the surface Σ at the locations of the foci.

(3) The flow on these unstable manifolds provides an orientation for the surface.

(4) The z axis (which was to be removed when constructing the handle-body as an embedding manifold) intersects the surface at one point.

Condition (3) forces the surface to be nonflat (twisted) as viewed in the embedding handle-body. When walking on one side of the surface Σ we see the flow going around both focal points in the same sense (let us say clockwise). Next we remove three points from the surface—the two focal points and the point of intersection with the z axis. This turns Σ into a genus-3 surface Ω. Consider a small circle in Ω, surrounding the just-removed point of intersection with the z axis. The induced one-dimensional flow along this circle will have four singularities that are alternately sources and sinks (joining and splitting points). They correspond in a formal way to the singularities in the branched manifold of the attractor—respectively to the branch lines and the splitting points. The surface Ω can be mapped one-to-one to a planar surface having the same genus, orientation, and the same number and type of singular points. This is represented in Fig. 4. Next we simplify the matter even further by introducing something that we call a canonical form. It is a planar surface with genus 3 in the case of the Lorenz attractor. The outside boundary is given an orientation. The inside boundary consists of three disjoint pieces—two circles and a square in between. The circles are provided with the same orientation as the outside boundary. The square is dressed with one-dimensional flow in such a way that the vertices of the square are alternately sources and sinks for the flow (cf. Fig. 3). The canonical form is a simplified representation of Ω and its flow singularities. There is a correspondence between these four objects—a chaotic attractor, an embedding manifold (with no fixed points inside), a branched manifold, and a canonical form. The relationship is illustrated as follows:

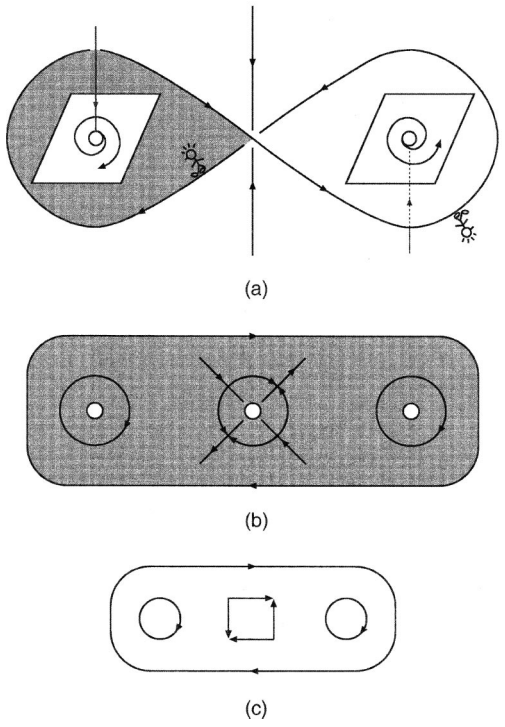

FIG. 4. (a) Two-dimensional genus three surface Ω that has an orientation induced by the flow around the focal points. (b) Planar equivalent of Ω indicating the singular set of the induced flow. (c) Canonical form.

$$\begin{array}{ccc} \text{Strange attractor} & \leftrightarrow & \text{Branched manifold} \\ \downarrow\downarrow\downarrow & & \downarrow\downarrow\downarrow \\ \text{Embedding manifold} & \leftrightarrow & \text{Canonical form.} \end{array}$$

This means that there is a 1-1 correspondence between strange attractors and branched manifolds (with a basis set of orbits). There is also a 1-1 correspondence between embedding manifolds and their canonical forms, up to smooth deformations. Many inequivalent strange attractors can be contained in the same embedding manifold. In the same way, many different branched manifolds can be enclosed by the same bounding torus. For example in Fig. 5 we show two different branched manifolds represented by the same canonical form.

IV. BOUNDING TORI AND CANONICAL FORMS

The boundary of the embedding manifold for a strange attractor in $\mathbb{R}^3$ is a union of closed orientable two-dimensional surfaces of genus $g \geqslant 1$. This boundary also en-

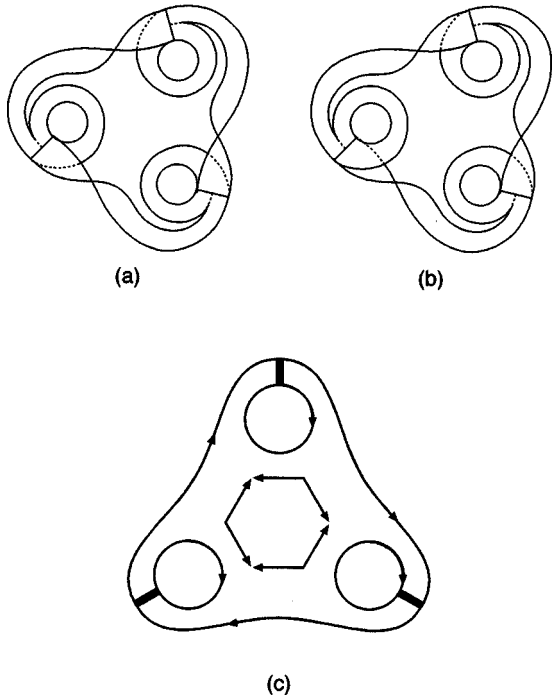

FIG. 5. (a) Branched manifold describing the three-fold cover of the Rössler system. (b) Branched manifold for attractor with no symmetry. (c) Canonical form for both systems.

closes the branched manifold since the unstable periodic orbits in the attractor are mapped to the branched manifold under the Birman-Williams projection. In that sense the branched manifold "sits" inside and is enclosed by the bounding torus. The flow for the original dynamical system that generates a strange attractor has $2(g-1)$ singularities when restricted to the genus-g surface. An algorithm for projecting these flow properties onto a planar surface (preceding section and Fig. 4) generates a disk with an outer boundary and g interior holes. The flow on the outer disk boundary is in a single direction (either clockwise or counterclockwise) without singularities. All singularities are distributed around the interior holes. The singularities occur in pairs. We call these (s,j) pairs, where an s-type singularity splits the flow and a j-type singularity occurs where flows from different regions join. Singularities of types s and j describe the nearby presence of splitting and joining charts in the embedded branched manifold. The distribution of singularities around the interior holes has a profound effect on the structure of the flow. We show holes with 0, 2, 4, and 6 singularities in Fig. 6. For the most part, holes separate the flow, as represented by the branched manifold, from the singularities in the vector field that generates the flow. The hole in Fig. 6(a) has no singularities. It separates a focus from the flow. The flow itself bears an imprint of this focus. The regular saddle shown in Fig. 6(c) induces four singularities on the hole surrounding it. This saddle also leaves its imprint on the structure of the flow in its neighborhood. The threefold degenerate saddle shown in Fig. 6(d) induces 2×3 singularities on the surrounding hole in the canonical form. This degenerate saddle also provides an unmistakable imprint on the structure of the neighboring flow in the interior of the embedding manifold.

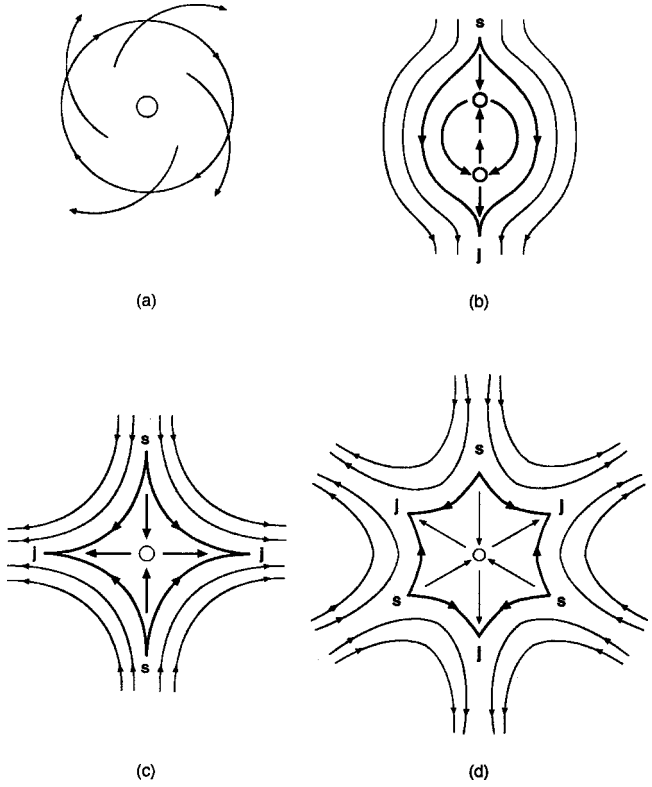

FIG. 6. Holes with (a) 0, (b) 2, (c) 4, and (d) 6 singularities. Only holes with two singularities can be removed without changing the asymptotic structure of the flow.

Holes supporting only one (s,j) pair of singularities do not have the same properties as holes with $0,4,6,\ldots$ singularities. As shown in Fig. 6(b) they do not leave an imprint on the surrounding flow. Such holes can be removed without changing the nature of the neighboring flow. They can be removed by "zipping them up" [13], that is, we identify the two boundaries connecting the s and j singularities.

Holes with two singularities can be encountered for a number of reasons. They are often drawn in representations of the standard Smale horseshoe branched manifold to allow easy distinction between the two branches. Such holes do not exist except in the hyperbolic limit, which has never been observed in experimental data, or even in numerical simulations of ordinary differential equations. Such holes can also be observed when large numbers of orbits have been pruned away. They can be observed in Rössler dynamics [14] and in the Shimizu-Morioka attractor for some parameter values. They are encountered in short data sets. They are also seen when invariant sets penetrate the flow (for example, placing your finger in a laminar fluid flow). This occurs, for example, when the Lorenz attractor is mapped to a Rössler-like attractor by modding out the symmetry [15]. They also occur around real or virtual saddle-node pairs, as shown in Fig. 6(b). In all instances, holes with two singularities can be (topologically) zipped up. The two singularities and the hole they are on disappear without changing the asymptotic properties of the flow.

As a result, interior holes without singularities can be regarded as circles and those with singularities as regular polygons with $4,6,8,\ldots$ sides.

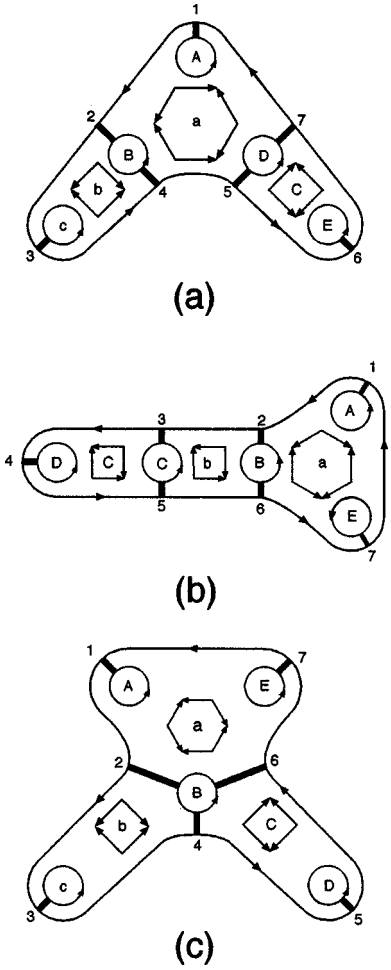

FIG. 7. Canonical forms corresponding to genus-8 bounding torus. They all have five circles, two squares, and one hexagon. The three forms are inequivalent—they are described by different periodic sequences: (a) abbacca, (b) abccbaa, and (c) abbccaa.

A canonical form for a bounding torus with genus 1 has one interior hole and no singularities anywhere. The flow on the exterior boundary and on the interior hole is in the same direction. A canonical form for a bounding torus with genus $g=2$ does not exist, since its Euler characteristic must be -2 and that condition cannot be satisfied by any combination of circles and polygons. Canonical forms for bounding tori with genus $g \geqslant 3$ have m interior circles and n interior polygons. The positive integers m and n obey

$$m + n = g, \tag{3}$$

$$m > n \geqslant 1, \tag{4}$$

where $n=1,2,\ldots,n_{MAX}$ and g is the genus. If the genus g is odd the maximum number of regular polygons is $n_{MAX}=m-1$. In the case of even genus g the upper bound is $n_{MAX}=m-2$. As is shown in Fig. 7 the genus itself is not enough to specify the canonical form. Even the combination (m,n) is not enough to specify uniquely the canonical form. For g sufficiently large $(g \geqslant 7)$ degeneracies occur.

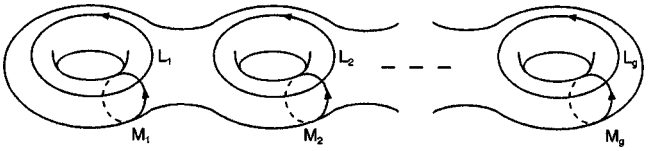

FIG. 8. Longitudes L_i and meridians M_i for a handle-body of genus g.

We should mention that most of the known strange attractors in three-dimensional phase space are created by the Smale horseshoe mechanism. As a result they all can be embedded in a solid torus with one hole. For those systems the canonical form is simply an annulus. For a torus with genus 1, the Euler characteristic χ is zero and the surface flow has no singularities.

In addition we want to mention a dynamical system for which the boundary of the embedding manifold is a union of two tori with genus 1—this is the velocity-driven Van der Pol system. The chaotic attractor shows an annular Poincaré surface of section. The boundary of the embedding manifold is a disjoint union of two tori of genus 1 each. The canonical form for this system is the union of two annuli.

One of the most important advantages in using canonical forms is in the way Poincaré surfaces of section are viewed. Next we provide some more insight in this direction.

V. POINCARÉ SURFACE OF SECTION

The most important characteristic of a Poincaré surface of section is that the flow crosses it transversally and always from the same side. This is in fact the most troublesome point when it comes to construction of such surfaces in practice. For a general flow it is not known whether we can always construct a Poincaré surface of section. The answer is positive for the particular kind of systems we are interested in: dissipative dynamical systems with $d_L<3$. We justify this assertion with the following considerations.

The simplest case is when the strange attractor can be embedded in a solid torus with no fixed points inside. The boundary is a two-torus. There are two generators of the fundamental group (the first homotopy group) $\pi_1(T^2)$ of the two-torus [16]. They represent two inequivalent classes of simple closed curves that cannot be shrunk to a point. The classes are inequivalent under smooth deformations. The simple closed curve that bounds a disk in the solid torus is called a meridian. We will call the other curve a longitude—it bounds a disk outside the solid torus and it serves as a generator of the fundamental group of the solid torus $\pi_1(D^2 \times S^1)$. In fact the notion of a longitude as applied usually to solid torus is a bit less restrictive (see Ref. [17] for details) but we use it provided no confusion will arise. The notions of longitudes and meridians can be extended to handle-bodies of higher genus. This is illustrated in Fig. 8. In the solid torus case we can always find a disk that is crossed transversally by the flow—namely, a disk bounded by a meridian. This disk serves as a Poincaré surface of section. The image of this disk under Birman-Williams projection and the branch line on the branched manifold can be identified. The

Poincaré map for these systems is thus represented in the canonical form representation by a mapping of intervals to intervals. There is another possible case—when we have a mapping of the circle onto itself. This occurs when the Poincaré surface of section has the topology of an annulus. This is the case with strange attractor of the velocity driven the Van der Pol oscillator (Birkhoff-Shaw attractor [18]).

For bounding tori with genus $g \geqslant 3$ we group the $2g-2$ singularities into $g-1$ pairs of (j,s) singularities. All branch lines must occur between a singularity of type j and the following (in the sense of the flow) singularity of type s. Branch lines between the same j and s type singularities can be consolidated into a single branch line by local moves [6]. This branch line can be moved to a disk that is transverse to the flow and between these two singularities. This disk is bounded by a meridian and forms one component of the global Poincaré surface of section. In this way we construct the global Poincaré surface of section for any flow whose canonical bounding torus has genus g. The Poincaré section is the union of $g-1$ disjoint disks, one disk between each (j,s) pair of singularities. Each disk contains one branch line of any branched manifold compatible with the canonical bounding torus.

In the canonical forms (see Fig. 7) we use $g-1$ intervals to show possible locations for the $g-1$ disks that are components of the Poincaré surface of section. These intervals simultaneously represent branch lines of any branched manifold enclosed by the bounding torus. All such intervals have one of their ends on the outside boundary and the other end on some circular internal boundary. It is clear that in general there will be one or more intervals connected to each circle. The exact location is determined so that there are exactly $g-1$ intervals connected to $m<g$ circles. There is no one-to-one mapping between the intervals, but rather one-to-two due to the splitting points in the template.

VI. TRANSITION MATRICES

An additional virtue of the canonical form representation is the ease with which one can introduce symbolic notation. This is done as follows. We choose an interval representing a component of the Poincaré surface of section. We put a numerical label 1 on it. Following the outside boundary in the direction of its orientation we number all the intervals in the order that they are encountered. Thus all intervals are labeled $1,2,3,\ldots,g-1$. Then we can construct a $(g-1)\times(g-1)$ matrix that represents how the intervals are mapped under the flow. We call this matrix a transition matrix. We provide an example for the canonical form in Fig. 7(a). Since the genus is 8 the transition matrix is 7×7.

$$T=\begin{pmatrix} 1 & 1 & 0 & 0 & 0 & 0 & 0 \\ 0 & 0 & 1 & 1 & 0 & 0 & 0 \\ 0 & 0 & 1 & 1 & 0 & 0 & 0 \\ 0 & 1 & 0 & 0 & 1 & 0 & 0 \\ 0 & 0 & 0 & 0 & 0 & 1 & 1 \\ 0 & 0 & 0 & 0 & 0 & 1 & 1 \\ 1 & 0 & 0 & 0 & 1 & 0 & 0 \end{pmatrix}.$$

The transition matrix has only 0's and 1's as entries. The presence of a 1 in location (i,j) means that initial conditions on the interval i can flow to interval j. Zero implies lack of such connection. There are only two 1's in each row (column). Note that elements $a_{12},a_{23},a_{34},a_{45},a_{56},a_{67},a_{71}$ are nonzero. This is due to the way we numbered the branch lines—going around the outer boundary and enumerating the intervals as we encounter them. It is convenient to split the transition matrix in two pieces—a cyclic part CL and a connectivity part CC. The sum of the two gives the transition matrix. All canonical forms with given genus g have the same cyclic matrix under the numbering convention introduced above. For example, for the forms in Fig. 7 the cyclic matrix has the seven nonzero elements listed above and is

$$\mathrm{CL}_8=\begin{pmatrix} 0 & 1 & 0 & 0 & 0 & 0 & 0 \\ 0 & 0 & 1 & 0 & 0 & 0 & 0 \\ 0 & 0 & 0 & 1 & 0 & 0 & 0 \\ 0 & 0 & 0 & 0 & 1 & 0 & 0 \\ 0 & 0 & 0 & 0 & 0 & 1 & 0 \\ 0 & 0 & 0 & 0 & 0 & 0 & 1 \\ 1 & 0 & 0 & 0 & 0 & 0 & 0 \end{pmatrix}.$$

The remaining part of the transition matrix shows the connectivity between the components of the Poincaré surface of section (represented by intervals) as due to the structure of the attractor. For example, for the canonical forms in Fig. 7 the connectivity matrices are, respectively,

$$\mathrm{CC}^1_{(5,3)}=\begin{pmatrix} 1 & 0 & 0 & 0 & 0 & 0 & 0 \\ 0 & 0 & 0 & 1 & 0 & 0 & 0 \\ 0 & 0 & 1 & 0 & 0 & 0 & 0 \\ 0 & 1 & 0 & 0 & 0 & 0 & 0 \\ 0 & 0 & 0 & 0 & 0 & 0 & 1 \\ 0 & 0 & 0 & 0 & 0 & 1 & 0 \\ 0 & 0 & 0 & 0 & 1 & 0 & 0 \end{pmatrix}=(2,4)(5,7),$$

$$\mathrm{CC}^2_{(5,3)}=\begin{pmatrix} 1 & 0 & 0 & 0 & 0 & 0 & 0 \\ 0 & 0 & 0 & 0 & 0 & 1 & 0 \\ 0 & 0 & 0 & 0 & 1 & 0 & 0 \\ 0 & 0 & 0 & 1 & 0 & 0 & 0 \\ 0 & 0 & 1 & 0 & 0 & 0 & 0 \\ 0 & 1 & 0 & 0 & 0 & 0 & 0 \\ 0 & 0 & 0 & 0 & 0 & 0 & 1 \end{pmatrix}=(2,6)(3,5),$$

$$\mathrm{CC}^3_{(5,3)}=\begin{pmatrix} 1 & 0 & 0 & 0 & 0 & 0 & 0 \\ 0 & 0 & 0 & 1 & 0 & 0 & 0 \\ 0 & 0 & 1 & 0 & 0 & 0 & 0 \\ 0 & 0 & 0 & 0 & 0 & 1 & 0 \\ 0 & 0 & 0 & 0 & 1 & 0 & 0 \\ 0 & 1 & 0 & 0 & 0 & 0 & 0 \\ 0 & 0 & 0 & 0 & 0 & 0 & 1 \end{pmatrix}=(2,4,6).$$

The lower index in the cyclic matrix name CL_8 shows the genus of the canonical form. The notation for the connectiv-

ity matrix name is of the form $CC^{i}_{(m,n)}$ where m is the number of circles, n is the number of regular polygons (with even number of sides) and i is a degeneracy index. The connectivity matrices can be expressed simply in terms of symmetric (permutation) group operations. They can be expressed as products of cycles [19]. These expressions are also given in Eqs. (5) above.

VII. CODING THE CANONICAL FORMS

Canonical forms can be labeled uniquely. The basic idea is that in a walk around the boundary in the direction of the flow the regular holes, the singular holes, and the branch lines are met in a systematic way. The way is coded by a sequence of $g-1$ symbols, repeated infinitely. In other words, the symbolic encoding of a canonical form is given by a "period $g-1$ orbit." The symbols can describe (1) the order in which the regular polygons are encountered between branch lines; (2) the order in which the circles without singularities are encountered at branch lines; (3) the number of branch lines attached to each circle without singularities, as the circles are encountered.

For example, for the canonical form shown in Fig. 7(a) the branch lines are labeled 1–7 in the order encountered. Starting from branch line 1, the polygons are encountered *a* first, then *b* (then *a* again), and *c*. The circles are encountered *A*, *B*, *C* (then *B*), *D*, *E* (and *D* again). The first circle encountered (*A*) has one branch line attached, *B* has two, *C* has 1, *B* has 2, *D* has 2, *E* has one, and *D* has 2. All these sequences repeat as one follows the flow around again past branch line 1. The three encodings are *abbacca*, *ABCBDED*, and 1212212. Since these results are invariant under cyclic permutation (i.e., change of starting point), it is useful to label each by some "lowest" word. For the canonical forms in Fig. 7 we obtain the following strings:

Sequence of Polygons	Sequence of Circles	Number of Intervals
aabbacc	*ABCBDED*	1212212
aaabccb	*ABCDCBE*	1221221
aaabbcc	*ABCBDBE*	1313131

The coding in the last column easily translates into the transition matrix for the canonical form. This is done as follows. A digit 1 in a particular position implies the existence of a period 1 orbit (a one cycle). A digit 2 occurs in pairs and it stands for a period 2 orbit. It forms a doublet. A digit 3 occurs in three places and denotes a three-cycle. It forms a triplet. Multiplets do not interleave. For example, there are two pairs of 2's in each of the first two rows of the third column. They stand for different period two orbits. We decipher the numerical string into the CC of the transition matrix as follows. First we write the string along the diagonal of a $(g-1)\times(g-1)$ matrix with all other entries equal to zero. We keep the digits 1 in place. Digits $n>1$ representing n cycles are shifted to the proper locations on the row and written there as 1. For example, in the first string we have a two-cycle represented by digit 2 in the second and the fourth positions. This means that in the connectivity matrix elements (2,4) and (4,2) will be 1. The procedure is illustrated below for the first numerical string:

$$\begin{pmatrix} 1&0&0&0&0&0&0\\ 0&2&0&0&0&0&0\\ 0&0&1&0&0&0&0\\ 0&0&0&2&0&0&0\\ 0&0&0&0&2&0&0\\ 0&0&0&0&0&1&0\\ 0&0&0&0&0&0&2 \end{pmatrix} \rightarrow \begin{pmatrix} 1&0&0&0&0&0&0\\ 0&0&0&1&0&0&0\\ 0&0&1&0&0&0&0\\ 0&1&0&0&0&0&0\\ 0&0&0&0&0&0&1\\ 0&0&0&0&0&1&0\\ 0&0&0&0&1&0&0 \end{pmatrix}.$$

Using this symbolic notation we can proceed to enumerate all canonical forms up to genus 9. This is done next.

VIII. ENUMERATION OF CANONICAL FORMS

To provide a complete classification of canonical forms we need to find a way to deal with degeneracy (cf, Fig. 7). This becomes important as the genus increases above 6. For that reason we propose a method that is reminiscent of the use of Young partitions to classify representations of permutation groups and Lie groups. The idea can be roughly described as follows. A genus $g=m+n$ canonical form will have $2g-2$ singularities located at the vertices of n even-sided regular polygons that are part of the internal boundary. In fact these singularities occur in pairs—sources and sinks (splitting and joining points). The problem reduces to finding a way to partition $g-1$ pairs into different sets of positive integers $\geqslant 2$. Each set has $p_i \geqslant 2$ members. Two pairs represent a square in the canonical form (a regular saddle), three pairs stand for a hexagon (threefold degenerate saddle), etc. We list the number of pairs in nonincreasing order and present them in the form $(p_1,p_2,p_3,\ldots,p_n)$, where the constraint is

$$p_1 \geqslant p_2 \geqslant p_3 \geqslant \cdots \geqslant p_n \geqslant 2, \quad \sum_{i=1}^{n} p_i = g-1.$$

Such partitions are not sufficient in some cases (as illustrated in Fig. 7). The degeneracy is lifted by using numerical strings: e.g., 1212212. The digit in each position of the numerical string represents the number of intervals connected to a circular hole encountered in a trip along the oriented disk's outer boundary. Examples of such numerical strings were shown in the preceding section. They also encode all the information about the transition matrix of the canonical form.

In Table I we enumerate canonical forms up to genus 9. We list the genus g, the number m of circular holes, the partition of the singularities, and the numerical string from which the connectivity matrix can be recovered. The numerical strings are unique up to a cyclic permutation.

TABLE I. Enumeration of canonical forms up to genus 9.

g	m	$(p_1,p_2,\ldots,p_n)$	$n_1n_2\ldots n_{g-1}$
1	1	(0)	1
3	2	(2)	11
4	3	(3)	111
5	4	(4)	1111
5	3	(2,2)	1212
6	5	(5)	11111
6	4	(3,2)	12112
7	6	(6)	111111
7	5	(4,2)	112121
7	5	(3,3)	112112
7	4	(2,2,2)	122122
7	4	(2,2,2)	131313
8	7	(7)	1111111
8	6	(5,2)	1211112
8	6	(4,3)	1211121
8	5	(3,2,2)	1212212
8	5	(3,2,2)	1221221
8	5	(3,2,2)	1313131
9	8	(8)	11111111
9	7	(6,2)	11111212
9	7	(5,3)	11112112
9	7	(4,4)	11121112
9	6	(4,2,2)	11122122
9	6	(4,2,2)	11131313
9	6	(4,2,2)	11212212
9	6	(4,2,2)	12121212
9	6	(3,3,2)	11212122
9	6	(3,3,2)	11221122
9	6	(3,3,2)	11221212
9	6	(3,3,2)	11311313
9	5	(2,2,2,2)	12221222
9	5	(2,2,2,2)	12313132
9	5	(2,2,2,2)	14141414

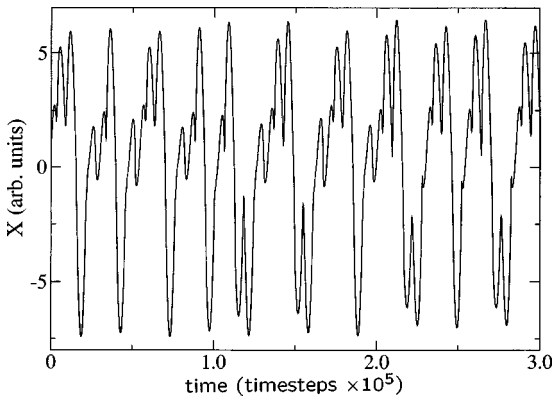

FIG. 9. Chaotic data set.

The number of inequivalent canonical forms $N(g)$ increases with g as follows:

g	$N(g)$
3	1
4	1
5	2
6	2
7	5
8	6
9	15

We speculate that this number increases exponentially with g: $N(g)\approx e^{hg}$. If true, it is possible to associate an "entropy" with canonical forms using the standard limiting definition:

$$h=\lim_{g\to\infty}\frac{\ln N(g)}{g}.$$

IX. ANALYSIS OF EXPERIMENTAL DATA

Once the branched manifold for a strange attractor has been determined it is relatively straightforward to find the corresponding canonical form. One drawback is that the topological analysis associated with the branched manifold determination is rather involved. For that matter it would be preferable if we can go directly from the experimental data to the canonical form. This can be done easily in lower genus cases. We provide a simple example.

In Fig. 9 we show a chaotic data set coming from a three-dimensional dynamical system. This is a numerically generated data set. It is also a generic data set.

Next we carry out a differential embedding of this data set in $\mathbb{R}^3$. In the reconstructed phase space with coordinates $(x(t),\dot{x}(t),\ddot{x}(t))$ we look at the projection in the $(x(t),\dot{x}(t))$ plane. This is shown in Fig. 10. One advantage of such a projection is that all the fixed points are located along the abscissa. Points in the upper half plane move to the right and points in the lower half plane move to the left. We see three fixed points around which the flow rotates one way. Thus we need at least three components for the Poincaré surface of section. Three components of the Poincaré surface of section are easily identified by inspection. They occur beyond points where flows from different circles join.

Next we look at how the sections are connected by the flow. With a little effort we see that the flow crossing section 1 is mapped either back to 1 or it goes to section 2. The flow crossing section 2 is mapped back to 2 or it is redirected to section 3. At section 3 a similar situation occurs—the flow either crosses again 3 or it is mapped to section 1 going along the band at the bottom of the projection. The transition matrix is

$$T=\begin{pmatrix}1&1&0\\0&1&1\\1&0&1\end{pmatrix}.$$

From this matrix we extract the following connectivity matrix:

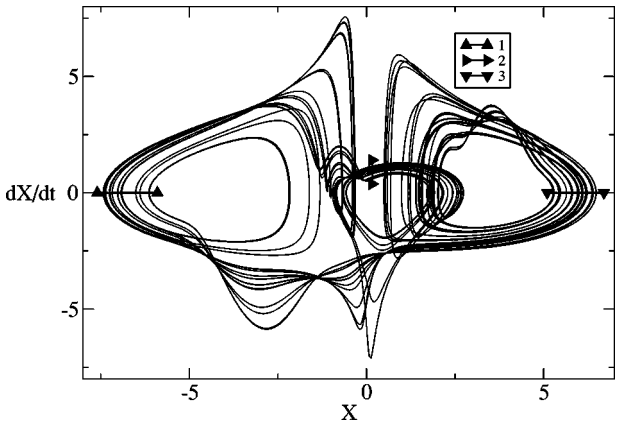

FIG. 10. Differential embedding of the data set shown in Fig. 8. The axes are $(x(t),\dot{x}(t))$. The fixed points are along the abscissa. The locations of suitably chosen components of the Poincaré surface of section are shown and numbered from 1 to 3, the first being the leftmost one.

$$C=\begin{pmatrix}1&0&0\\0&1&0\\0&0&1\end{pmatrix}.$$

This means that we have a cyclic configuration and the best candidate for a canonical form is the one corresponding to genus 4 in Table I. The only other possible choice (since $m=3$, $n=1$ or $n=2$ only) is the form that has genus 5 and three circles (three focal points and two saddles). However, this requires another component for the Poincaré surface of section to be associated with one of the holes in the attractor. Upon careful examination we see that there is no location where we can put another such component and not have a one-to-one mapping by the flow. Thus the right choice is the genus-4 canonical form. This form is presented graphically in Fig. 5(c). We would like to emphasize that from our analysis we cannot conclude that the branched manifold associated with our system is the one in Fig. 5(a) or 5(b). We do not know at this stage the number of branches or the way they are connected to the branch lines. This follows from the fact that the canonical form does not uniquely determine the branched manifold. It rather serves as an organizer indicating the number of singular sets and places constraints on the connectivity between branches. An additional constraint is put on the way branches fold when parameter values are changed—branches connecting to the same branch line but coming from different "tubes" in the embedding manifold must fold so that they do not intersect each other (see Ref. [1]).

In fact the data set for our example actually came from a threefold cover of the Rössler system. A numerically computed solution approaching a strange attractor is presented in Fig. 11. We plot only a projection on the *XY* plane since the cover was constructed by applying rotation about the *z* axis. The generic data set in Fig. 9 is a linear combination

$$-x(t)\sin(\phi)+y(t)\cos(\phi),$$

where the angle ϕ was chosen so that there is a large separation between the unstable foci. If we take the $x(t)$ variable

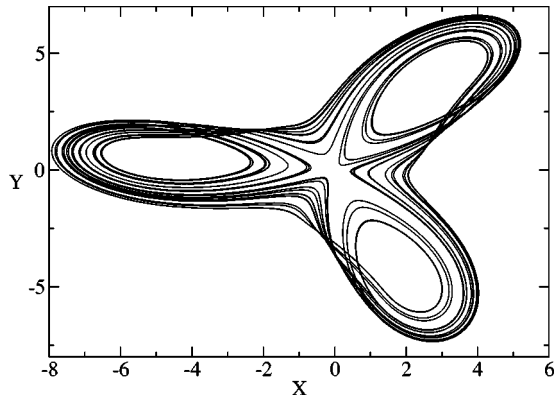

FIG. 11. A projection on the *XY* plane of the strange attractor of the threefold cover of the Rössler system.

$(\phi=3\pi/2)$, two of the fixed points will be nearly degenerate in the differential embedding.

X. DISCUSSION

We believe that the classification scheme in terms of canonical forms presented in this paper is an important advance in our understanding of low-dimensional chaos. The interplay between topology and dynamics leads to the appearance of a rich variety of possible structures for chaotic attractors. So far very little of this variety has been seen in practice—most strange attractors in $\mathbb{R}^3$ live inside a solid torus. Such lack of variety is due probably to the way nature works at this level—simple structures are abundant and complicated ones are rare. It could also be due to the fact higher genus attractors are difficult to model with analytic flows. Multispiral attractors have been modeled by nonanalytic, piecewise linear forcing functions [20].

Apart from the obvious use for classification purposes, our approach can be extended in at least two other different directions. First, the possible changes in the structure of a strange attractor as parameter values are varied can be explored. Apart from the constraint on the way branches fold, previously mentioned, many more interesting observations can be made. Second, starting from the transition matrix of the canonical form we can construct a set of coupled one-dimensional maps of the interval representing the mapping between components of the Poincaré surface of section after Birman-Williams projection has been applied [15]. The study of such maps will shed some light on orbit forcing in strange attractors with more complicated structure.

In addition we would like to mention that we did not consider any complications due to nontrivial (extrinsic) embedding of the handle-bodies in $\mathbb{R}^3$. Such situations occur, for example, if some of the handles are linked. The question of whether it is possible for a strange attractor to live inside such handle-body, and what impact this will have on its structure, requires further investigation.

ACKNOWLEDGMENTS

We thank G. Byrne for useful discussions. This work was partially supported by NSF Grant No. PHY 9987468.

[1] T. D. Tsankov and R. Gilmore, Phys. Rev. Lett. **91**, 134104 (2003).
[2] H. G. Solari and R. Gilmore, Phys. Rev. A **37**, 3096 (1988).
[3] N. B. Tufillaro, H. G. Solari, and R. Gilmore, Phys. Rev. A **41**, 5717 (1990).
[4] G. B. Mindlin, R. Lopez-Ruiz, H. G. Solari, and R. Gilmore, Phys. Rev. E **48**, 4297 (1993).
[5] R. Gilmore, Rev. Mod. Phys. **70**, 1455 (1998).
[6] R. Gilmore and M. Lefranc, *The Topology of Chaos* (Wiley, New York, 2002).
[7] J. Birman and R. F. Williams, Contemp. Math. **20**, 1 (1983).
[8] H. Poincaré, *Les Methodes Nouvelles de la Mécanique Celeste* (Gauthier-Villars, Paris, 1899).
[9] D. Sciamarella and G. B. Mindlin, Phys. Rev. Lett. **82**, 1450 (1999).
[10] D. Sciamarella and G. B. Mindlin, Phys. Rev. E **64**, 036209 (2001).
[11] E. N. Lorenz, J. Atmos. Sci. **20**, 130 (1963).
[12] V. Guillemin and A. Pollack, *Differential Topology* (Prentice-Hall, Englewood Cliffs, New Jersey, 1974).
[13] J. Weeks, *The Shape of Space* (Marcel Dekker, New York, 2002).
[14] J. M. T. Thompson and H. B. Stewart, *Nonlinear Dynamics and Chaos* (Wiley, New York, 2002).
[15] R. Gilmore and C. Letellier (unpublished).
[16] M. Nakahara, *Geometry, Topology and Physics* (IOP Publishing, Bristol, 1990).
[17] D. Rolfsen, *Knots and Links* (Publish or Perish, Berkeley, 1976).
[18] R. Shaw, Z. Naturforsch. A **36A**, 80 (1981).
[19] M. Hamermesh, *Group Theory and its Application to Physical Problems* (Dover, New York, 1989).
[20] M. A. Aziz-Alaoui, Int. J. Bifurcation Chaos Appl. Sci. Eng. **9**, 1009 (1999).